Annuaire de l'Université de Sofia "St. Kliment Ohridski", Faculté de Physique, 96, 2003

PARALLEL PROPAGATION OF SURFACE HALL-MHD WAVES ALONG AN IDEAL FLOWING PLASMA SLAB BOUNDED BY FLOWING PLASMA ENVIRONMENT

ROSSITSA MITEVA, IVAN ZHELYAZKOV

Department of Radiophysics and Electronics

Росица Митева, Иван Желязков. ПАРАЛЕЛНО РАЗПРОСТРАНЕНИЕ НА ПОВЪРХНИННИ ХОЛОВИ МХД ВЪЛНИ В ИДЕАЛЕН ТЕЧАЩ ПЛАЗМЕН СЛОЙ В ТЕЧАЩА ПЛАЗМЕНА СРЕДА

Изследва се паралелното разпространение (по направление на външното магнитно поле) на магнитохидродинамични (МХД) повърхнинни вълни по идеален течащ плазмен слой, намиращ се в течаща плазмена среда, в приближение на холовата магнитохидродинамика. Стойностите на плазмените скорост и плътност вътре и вън от слоя са различни. Разглеждат се две възможни посоки на относителната скорост (в координатна система, свързана с външния поток). Включването на постоянен поток вън от слоя променя дисперсионните характеристики на повърхнинните вълни, разпространяващи се по течащия слой, в сравнение със случая, когато външната среда е неподвижна. От двата вида повърхнинни вълни, които могат да се разпространяват в слоя, а именно *sausage* и *kink*, дисперсионното поведение на kink-мода по посока на относителната скорост се оказва много по-сложно, отколкото онова на sausage-мода.

Rossitsa Miteva, Ivan Zhelyazkov. PARALLEL PROPAGATION OF SURFACE HALL-MHD WAVES ALONG AN IDEAL FLOWING PLASMA SLAB BOUNDED BY FLOWING PLASMA ENVIRONMENT

The parallel propagation of magnetohydrodynamic (MHD) surface waves along an ideal flowing plasma slab, bounded by flowing plasma environment in the Hall magnetohydrodynamics approach is investigated. The magnitudes of the plasma velocity and density inside and outside the slab are different. Two possible directions of the relative velocity (in a frame of reference co-moving with the ambient flow) are considered. The inclusion of the steady flow outside the slab changes the dispersion characteristics of the surface waves travelling along the flowing slab in comparison with the case when the external medium is at rest. From the two kind surface wave modes that may occur, notably *sausage* and *kink*, the dispersion behaviour of the kink mode along the relative flow turns out to be much more complex than that of the sausage mode.

Keywords: Hall-MHD waves, solar-wind plasma, flow-tube structures
PACS numbers: 52.35.Bj; 96.50.Ci

INTRODUCTION

It is already confirmed by the HELIOS spacecrafts that the solar wind is fine-structured, consisting of the so-called 'spaghetti structures', i.e. thin, coherent flow-sheets (or tubes) that are adjacent to each other with differences in their plasma parameters (such as density and flow velocity), as it was first proposed by Parker [1]. Thus the study of the possible low-frequency wave modes that can be sustained by such structures is a current problem of the research in the solar astrophysics. As is well-known, there are three general type of waves (slow, intermediate or Alfvén and fast modes) that may exist in an infinite MHD plasma. The foregoing modes however do occur in bounded plasmas as well. The Hall-MHD theory, that may be used in recovering the characteristics of the different wave modes, relaxes the frequency limit of the ordinary MHD approach, widening the Hall-MHD range up to the ion-cyclotron frequency ω_{ci}. Moreover, a suitable Hall-MHD mode filter is need to be constructed in order to identify the different plasma waves contributed to the signals detected by satellites [2]. Satellite measurements of the solar wind characteristics (the magnetic field, the velocity and plasma density) are important to understand which plasma wave modes from the great variety of possible plasma waves do really occur.

Generally speaking, the Hall-MHD theory is relevant to plasma dynamics occurring on length scales shorter than an ion inertial length, $L < l_{\mathrm{Hall}} = c/\omega_{pi}$ (where c is the speed of light and ω_{pi} is the ion plasma frequency), and time scales shorter than an ion-cyclotron period, i.e. $t < \omega_{ci}^{-1}$ [3]. Assuming that the solar wind plasma is structured owing not only to different plasma/mass densities [4], but also due to different flow velocities inside and outside the slab, the Hall length for a solar wind flux tube at 1 AU within the chosen field parameters [notably ambient magnetic field $B_0 = 5 \times 10^{-9}$ T (and accordingly ion-cyclotron frequency $\omega_{ci}/2\pi = 0.076$ Hz), electron number density $n_e = 3 \times 10^6$ m^{-3}, electron temperature $T_e = 2 \times 10^5$ K] is $l_{\mathrm{Hall}} = 134$ km. This scale length is smaller than, but not negligible compared to the layer's width of a few hundred kilometers. The Alfvén speed inside and outside the slab is 64 km s^{-1} and 100 km s^{-1}, respectively, and the sound speed is 57 km s^{-1} inside and 89 km s^{-1} outside the slab.

The aim of this study is to investigate the Hall-MHD plasma modes that may propagate along an ideal plasma slab bounded by a distinct plasma environment including different flows in both compressible media. In the first case considered in the present work, the flow inside the slab is faster than the one of the surrounding plasma—as we consider parallel propagation, we take both velocities to be in the positive z-direction. Thus the direction of the corresponding relative velocity is forward (i.e. positive, outwards the Sun). When the two flow velocities are interchanged in magnitude, the relative flow velocity becomes negative or backward (i.e. towards the Sun). For each of the two above cases, one observes both forward ($\boldsymbol{k} = k\hat{z}$) and backward ($\boldsymbol{k} = -k\hat{z}$) sausage and kink waves [5]. The all eight possible waves' dispersive diagrams are presented.

BASIC EQUATIONS AND BOUNDARY CONDITIONS

Consider a flowing plasma slab of uniform density $\rho_{\rm o}$, flow velocity $\boldsymbol{U}_{\rm o}$ and thickness $2x_0$, bounded by flowing plasmas each with a density $\rho_{\rm e}$ and a flow velocity $\boldsymbol{U}_{\rm e}$, the interfaces being the surfaces $x = \pm x_0$. The uniform magnetic field $\boldsymbol{B}_0$ that is extended in both media and the two flow velocities point in the z direction. The wave vector $\boldsymbol{k}$ lies also along the z axis and its direction is the same as that of $\boldsymbol{B}_0$ for forward waves and opposite for backward waves, respectively. The basic equations for Hall-MHD waves are the following linearized equations governing the evolution of perturbed plasma density $\delta\rho$, pressure δp, fluid velocity $\delta\boldsymbol{U}$ and the wave magnetic field $\delta\boldsymbol{B}$ [6]:

$$\frac{\partial}{\partial t}\delta\rho + (\boldsymbol{U}_0\cdot\nabla)\delta\rho + \rho_0\,\nabla\cdot(\delta\boldsymbol{U}) = 0, \tag{1}$$

$$\rho_0\frac{\partial}{\partial t}\delta\boldsymbol{U} + \rho_0(\boldsymbol{U}_0\cdot\nabla)\delta\boldsymbol{U} + \nabla(\delta\rho + \frac{1}{\mu_0}\boldsymbol{B}_0\cdot\delta\boldsymbol{B}) - \frac{1}{\mu_0}(\boldsymbol{B}_0\cdot\nabla)\delta\boldsymbol{B} = 0, \tag{2}$$

$$\nabla\cdot\delta\boldsymbol{B} = 0, \tag{3}$$

$$\frac{\partial}{\partial t}\delta\boldsymbol{B} - (\boldsymbol{B}_0\cdot\nabla)\delta\boldsymbol{U} + \boldsymbol{B}_0\nabla\cdot(\delta\boldsymbol{U}) + (\boldsymbol{U}_0\cdot\nabla)\delta\boldsymbol{B} + l_{\rm Hall}\frac{v_{\rm A}}{B_0}\boldsymbol{B}_0\cdot\nabla\nabla\times\delta\boldsymbol{B} = 0, \tag{4}$$

$$\frac{\partial}{\partial t}\delta p + (\boldsymbol{U}_0\cdot\nabla)\delta p + \gamma p_0\nabla\cdot\delta\boldsymbol{U} = 0, \tag{5}$$

where the ratio of specific heats is set $\gamma = 5/3$ for a monoatomic gas, the Alfvén velocity is $v_{\rm A} = B_0/(\mu_0\rho_0)^{1/2}$ and $l_{\rm Hall} = v_{\rm A}/\omega_{ci}$ (which is equivalent to c/ω_{pi}). Here all quantities with subscript zero refer to equilibrium values. The pressure perturbation δp is related to the mass density perturbation $\delta\rho$ via $\delta p = v_s^2\delta\rho$, where $v_s = (\gamma p_0/\rho_0)^{1/2}$ is the sound speed. Equations (1) through (5) can be Fourier transformed, assuming that all perturbed quantities are of the kind $\propto g(x)\exp(-i\omega t + ikz)$, i.e. $\partial/\partial t = -i\omega$, $\partial/\partial x \neq 0$, $\partial/\partial y = 0$, $\partial/\partial z = ik$. Following the same procedure as in Ref. [6], we derive the two coupled second order differential equations for $\delta U_x(x)$ and $\delta U_y(x)$:

$$\left(\frac{d^2}{dx^2} - Ak^2\right)\delta U_x - i\frac{a-1}{\varepsilon}Ak^2\delta U_y = 0, \tag{6}$$

$$\left(\frac{d^2}{dx^2} - q^2\right)\delta U_x + i\frac{\varepsilon}{a-1}\frac{q^2}{k^2}\left(\frac{d^2}{dx^2} - k^2\right)\delta U_y = 0, \tag{7}$$

where

$$\varepsilon = \frac{\omega - \boldsymbol{k}\cdot\boldsymbol{U}_0}{\omega_{ci}}, \qquad a = \frac{(\omega - \boldsymbol{k}\cdot\boldsymbol{U}_0)^2}{k^2 v_{\rm A}^2}, \qquad A = \frac{a}{1 + (a-1)k^2/q^2},$$

$$q^2 = \frac{[(\omega - \boldsymbol{k}\cdot\boldsymbol{U}_0)^2 - k^2 v_{\mathrm{A}}^2][(\omega - \boldsymbol{k}\cdot\boldsymbol{U}_0)^2 - k^2 v_s^2]}{k^2 v_{\mathrm{A}}^2 v_s^2 - (\omega - \boldsymbol{k}\cdot\boldsymbol{U}_0)^2(v_{\mathrm{A}}^2 + v_s^2)}.$$

We are seeking the solutions to the coupled Eqs. (6) and (7) in the form

$$\delta U_x(x) = f[\exp(-\kappa x) \mp \exp(\kappa x)],$$

$$\delta U_y(x) = ih[\exp(-\kappa x) \mp \exp(\kappa x)].$$

With these expressions for δU_x and δU_y one obtains a homogeneous set of equations for the amplitudes f and h and in order to get nontrivial solutions to them the attenuation coefficient κ has to obey the bi-quadratic equation

$$\kappa^4 - k^2 \left[1 + A\left(1 - \left(\frac{k}{q}\frac{a-1}{\varepsilon}\right)^2\right)\right]\kappa^2 + Ak^4\left[1 - \left(\frac{a-1}{\varepsilon}\right)^2\right] = 0, \qquad (8)$$

which solution has the form

$$\kappa_{1,2} = \frac{k}{\sqrt{2}}\left\{1 + A\left[1 - \left(\frac{k}{q}\frac{a-1}{\varepsilon}\right)^2\right]\right.$$

$$\left.\pm\sqrt{\left\{1 + A\left[1 - \left(\frac{k}{q}\frac{a-1}{\varepsilon}\right)^2\right]\right\}^2 - 4A\left[1 - \left(\frac{k}{q}\frac{a-1}{\varepsilon}\right)^2\right]}\right\}^{1/2}. \qquad (9)$$

This means that we have in fact *two* pairs of attenuation coefficients, notably $(\kappa_{\mathrm{o}1}, \kappa_{\mathrm{o}2})$ inside the slab and $(\kappa_{\mathrm{e}1}, \kappa_{\mathrm{e}2})$ outside the slab.

As is known, a bounded MHD plasma flux tube (cylinder or layer) could sustain two types of waves—*sausage* and *kink* modes. In the particular case of slab geometry the general solutions to the governing set of Eqs. (6,7) are sought as a superposition of $\sinh\kappa_{\mathrm{o}}x$ for the sausage mode and $\cosh\kappa_{\mathrm{o}}x$ for the kink mode, both inside the slab, and as a superposition of exponents of $\kappa_{\mathrm{e}}x$—outside the layer. So the solutions for the sausage mode inside the layer ($|x| < 0$) can be presented in the following form

$$\delta U_x(x) = f_1\frac{\sinh\kappa_{\mathrm{o}1}x}{\sinh\kappa_{\mathrm{o}1}x_0} + f_2\frac{\sinh\kappa_{\mathrm{o}2}x}{\sinh\kappa_{\mathrm{o}2}x_0},$$

$$\delta U_y(x) = if_1G_{\mathrm{o}1}\frac{\sinh\kappa_{\mathrm{o}1}x}{\sinh\kappa_{\mathrm{o}1}x_0} + if_2G_{\mathrm{o}2}\frac{\sinh\kappa_{\mathrm{o}2}x}{\sinh\kappa_{\mathrm{o}2}x_0}.$$

The solutions for the kink mode are the same as for the sausage wave but instead of sinh there appears the cosh function. The solutions outside the slab for $x > x_0$ are

$$\delta U_x(x) = \alpha_1\exp[-\kappa_{\mathrm{e}1}(x - x_0)] + \alpha_2\exp[-\kappa_{\mathrm{e}2}(x - x_0)],$$

$$\delta U_y(x) = i\alpha_1G_{\mathrm{e}1}\exp[-\kappa_{\mathrm{e}1}(x - x_0)] + i\alpha_2G_{\mathrm{e}2}\exp[-\kappa_{\mathrm{e}2}(x - x_0)],$$

and

$$\delta U_x(x) = \beta_1 \exp[\kappa_{\mathrm{e}1}(x + x_0)] + \beta_2 \exp[\kappa_{\mathrm{e}2}(x + x_0)],$$
$$\delta U_y(x) = i\beta_1 G_{\mathrm{e}1} \exp[\kappa_{\mathrm{e}1}(x + x_0)] + i\beta_2 G_{\mathrm{e}2} \exp[\kappa_{\mathrm{e}2}(x + x_0)],$$

for $x < -x_0$, respectively, where all fs, indexed αs and βs represent the amplitudes of the corresponding wave mode and

$$G_{1,2} = -\frac{\varepsilon}{A(a-1)} \frac{\kappa_{1,2}^2 - Ak^2}{k^2}.$$

It is worth stressing that the coefficients $G_{1,2}$ together with ε, a, q and A possess different values inside and outside the layer, which as well as all the other similar quantities in the paper (for example $\kappa_{1,2}$), are written down correspondingly with subscripts 'o' and 'e'.

All other perturbed quantities such as the total pressure $\delta p_{\mathrm{total}}$ (gas + magnetic) and electric field components δE_x and δE_y, which will be used in the boundary conditions, are expressed in terms of δU_x and δU_y and their forms correspondingly are:

$$\delta p_{\mathrm{total}} = i\frac{\rho_0}{\omega - \boldsymbol{k}\cdot\boldsymbol{U}_0} v_{\mathrm{A}}^2 \left\{ \frac{k^2}{q^2} \left[\frac{(\omega - \boldsymbol{k}\cdot\boldsymbol{U}_0)^2}{k^2 v_{\mathrm{A}}^2} - 1 \right] \frac{d}{dx}\delta U_x + i\varepsilon \frac{d}{dx}\delta U_y \right\},$$

$$\delta E_x = -\frac{\omega}{\omega - \boldsymbol{k}\cdot\boldsymbol{U}_0} \left(\frac{\omega - \boldsymbol{k}\cdot\boldsymbol{U}_0}{k v_{\mathrm{A}}} \right)^2 B_0 \delta U_y,$$

and

$$\delta E_y = \frac{\omega}{\omega - \boldsymbol{k}\cdot\boldsymbol{U}_0} B_0 \left[\delta U_x - i\frac{\omega - \boldsymbol{k}\cdot\boldsymbol{U}_0}{\omega_{ci}} \delta U_y \right].$$

The last two expressions have been derived from the generalized Ohm's law for the perturbed wave electric field

$$\delta\boldsymbol{E} = -\delta\boldsymbol{U} \times \boldsymbol{B}_0 - \boldsymbol{U}_0 \times \delta\boldsymbol{B} - l_{\mathrm{Hall}} \frac{v_{\mathrm{A}}}{B_0} \boldsymbol{B}_0 \times \nabla \times \delta\boldsymbol{B}.$$

As seen from the solutions to the basic Eqs. (6,7) the number of the integration constants is six. However, because of the symmetry (or antisymmetry) of the problem, the $\beta_{1,2}$ amplitudes are directly obtainable from the $x > x_0$ solutions, i.e. indexed αs and βs are not independent. Thus we can derive the dispersion relation by applying the boundary condition only at one interface, say $x = x_0$.

Usually the boundary conditions are obtainable by integrating the basic equations across the interfaces [6]. For our case of a flowing Hall-MHD structured plasma layer however the well-known boundary condition for continuity of the normal perturbed velocity δU_x has to be replaced by the one for continuity of the interface [7] $\delta U_x/(\omega - \boldsymbol{k}\cdot\boldsymbol{U}_{\mathrm{o,e}})$. The remaining boundary conditions are the continuity of the perturbed total pressure $\delta p_{\mathrm{total}}$ and the continuity of the y-component of perturbed wave electric field δE_y, and the x-component of perturbed electric displacement

$$\delta D_x = \varepsilon_0 (K_{xx}\delta E_x + K_{xy}\delta E_y),$$

where

$$K_{xx} \approx \frac{c^2}{v_{\mathrm{A}}^2} \quad \text{and} \quad K_{xy} \cong i\frac{\omega - \boldsymbol{k}\cdot\boldsymbol{U}_0}{\omega_{ci}}\frac{c^2}{v_{\mathrm{A}}^2}$$

are the low-frequency components of the plasma dielectric tensor [8].

DISPERSION RELATION AND NUMERICAL RESULTS

After applying the boundary conditions only at the one interface (doing the same on the other one would give the same results) we derive the dispersion relation of Hall-MHD sausage and kink surface waves that is presented symbolically in the form:

$$\mathcal{D}\left(\omega, k, U_{\mathrm{o}}, U_{\mathrm{e}}, B_0, x_0, \beta, \rho_{\mathrm{o}}, \rho_{\mathrm{e}}, l_{\mathrm{Hall}}\right) = 0. \tag{10}$$

We note that the dispersion relation for the sausage mode contains the function coth, while that for the kink mode—the function tanh (see the APPENDIX). When we take the limit of evanescent flow velocities, one gets dispersion relation (17) of Ref. [6]. Moreover, when the Hall term is neglected, dispersion relations (10) coincide with those obtained by Edwin and Roberts [9]. Dispersion relations for the sausage and kink modes are transcendental and can be solved only numerically. Before starting the procedure for finding the roots of (10), all entering quantities need to be suitably normalized with respect to the Alfvén speed inside the layer v_{Ao} and the semi-width of the slab x_0 and hence transformed to dimensionless quantities. Furthermore, in both dispersion relations the plasma and slab characteristics must be considered as entry parameters, and hence, specified before the start of equations' numerical solving.

The entry parameters for the current problem according to aforementioned plasma and slab characteristics are: the ratio of the densities inside and outside the slab $\rho_{\mathrm{o}}/\rho_{\mathrm{e}} = 2.44$, the plasma beta $\beta = 2\mu_0 n_e k_{\mathrm{B}} T_e/B_0^2 \approx (v_{s\mathrm{o}}/v_{\mathrm{Ao}})^2 = 0.79$, the ratio of the Hall length to x_0, i.e. $l_{\mathrm{Hall}}/x_0 = 0.4$, and the Alfvénic Mach numbers M_{o} and M_{e}, inside and outside the slab, respectively. The Alfvénic Mach number M is the ratio of a given flow velocity to the corresponding Alfvén velocity—M may vary from 0 (static state) up to 8 (for real solar-wind speeds). The choice for the value of $\rho_{\mathrm{o}}/\rho_{\mathrm{e}}$ cannot be arbitrary, but is defined by the constraint [6]

$$\frac{\rho_{\mathrm{e}}}{\rho_{\mathrm{o}}} = \frac{2v_{s\mathrm{o}}^2 + \gamma v_{\mathrm{Ao}}^2}{2v_{s\mathrm{e}}^2 + \gamma v_{\mathrm{Ae}}^2}, \tag{11}$$

which in the case of $B_0 = \mathrm{const}$ in the entire domain of interest is equivalent to

$$\frac{v_{s\mathrm{e}}^2}{v_{\mathrm{Ao}}^2} = \frac{\rho_{\mathrm{o}}}{\rho_{\mathrm{e}}}\frac{v_{s\mathrm{o}}^2}{v_{\mathrm{Ao}}^2},$$

implying that the plasma β should be equal in both media.

The magnitude of the ratio $l_{\rm Hall}/x_0$ depends on the width of the structure that could be described by the developed model. For typical values of a few hundred kilometers of the flow-structures in the solar-wind plasma and with the aforementioned Hall length, the chosen number of 0.4 seems to be adequate to the reality. The range of the values of both Alfvénic Mach numbers depends on the specified flow velocity for each of the investigated cases and generally starts from 0 (static plasma) up to 7–8 (for the case of slow-flowing streams in the solar wind). We allow the Mach numbers to be spread on a wide range of possible values, because the solar wind itself does not possess an exact magnitude, but swings around several typical values (generally one distinguishes fast- and slow-streams structures, originated from open and close magnetic line configurations, respectively [10]). All dispersion diagrams are presented as a dependence of the normalized wave's phase velocity $v_{\rm ph}/v_{\rm Ao}$ (where ω/k is the Doppler-shifted both inside and outside the slab wave phase velocity) on the dimensionless wave number kx_0 (or $|k|x_0$ with backward wave propagation). All dispersion curves are plotted by a step of 0.5 of the internal Alfvénic Mach number (and accordingly 0.28 for the forward-flow case and 0.365 for the backward-flow case of the external Alfvénic Mach number), while in the regions, corresponding to real flow velocities the step is diminished five times.

FORWARD FLOW

For a flowing plasma one can distinguish two kinds of waves: forward and backward with respect to the direction of the relative flow velocity (the difference between the two flow velocities or equivalently when one considers a frame of reference that is co-moving with the ambient flow). When the direction of the relative flow velocity is the same as the direction of the magnetic field (i.e. parallel to the z axis), the flow is called *forward* and vice versa. Starting with the case of a forward flow, we specify the flow velocity inside the layer to be $U_{\rm o} = 480\ {\rm km\,s^{-1}}$ and the one outside the layer—$U_{\rm e} = 420\ {\rm km\,s^{-1}}$ (or in terms of internal and external Alfénic Mach numbers—$M_{\rm o} = 7.5$ and $M_{\rm e} = 4.2$, respectively). The relative flow speed is $60\,{\rm km\,s^{-1}}$. With the so chosen values of the flow velocities it becomes apparent that we are going to deal with relatively slow moving flow structures that are mostly present in the ecliptic plane. Although the flow is chosen to be forward, still there are two possible directions of the wave to propagate, namely forward waves (with their wave vector lying in the same direction as the relative flow velocity) and backward waves [5] (with oppositely directed wave vector and flow velocity). Bearing in mind that in a bounded plasma the waves are distinguished to sausage and kink ones, finally we have four different cases to study: forward and backward sausage and forward and backward kink modes, all of them propagating in a forward flow.

Sausage waves in a forward flow

Here we discus the forward and backward sausage modes in a forward flow.

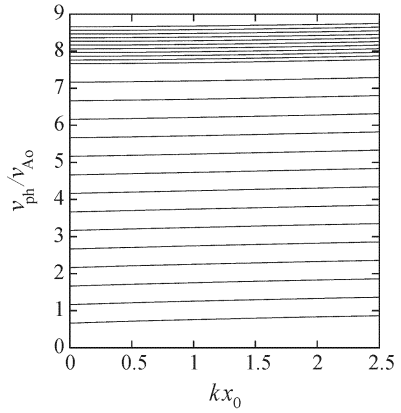

Fig. 1. Dispersion curves of forward sausage waves in a forward flow for $\beta = 0.79$, $\rho_o/\rho_e = 2.44$, $l_{Hall}/x_0 = 0.4$, $M_o = 0$–8, $M_e = 0$–4.48. The curves lying in the interval 0–7 are plotted by a step of 0.5 while in the range of 7–8 the $\Delta M_o = 0.1$

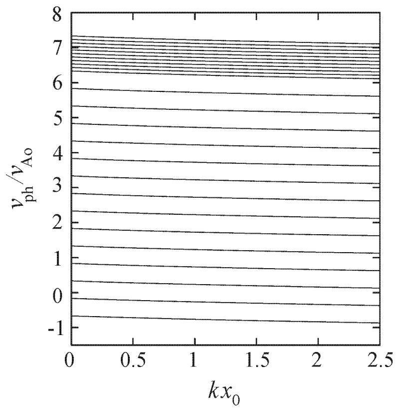

Fig. 2. Dispersion curves of backward sausage waves in a forward flow for the same parameters' set as in Fig. 1

In Fig. 1 we present the dispersion diagram for the forward sausage mode, whilst in Fig. 2 we show the dispersion curves for the backward sausage wave. In all figures presented the first curve at the bottom of the plot corresponds to a static flow slab ($M_{o,e} = 0$). Looking at Fig. 2, one sees that the normalized phase velocity (around 7) of the backward wave is diminished compared with the phase velocity of the forward wave for the same Mach numbers. Moreover, the waves are *actually* backward only for very small Mach numbers. With increasing the flow speed, the normalized phase velocity becomes positive, i.e. the wave is advected with the flow and continues to propagate in positive direction. Another distinction between the two families of dispersion curves is that those plotted in Fig. 1 present almost non-dispersive waves, whereas in Fig. 2 one observes for backward waves a reduced phase velocity in the short wavelength limit.

Kink waves in a forward flow

The dispersion curves of forward and backward kink waves are shown in Figs. 3, 4 and 5, respectively. We notice that the dispersion characteristics of the forward kink waves appear to be quite complex. The complexity occurs in the range of the v_{vh}/v_{Ao} between 7.2 and 9.2 (as is zoomed in Fig. 4). For each run of the numerical code for solving the corresponding dispersion relation in that phase-velocity range, there have been found more than three sets of roots (i.e. curves). The curve corresponding to $M_o = 6.5$ ($M_e = 3.64$) consists of three parts: the one part is visible at very small normalized wave numbers, while the remaining two parts merge at $kx_0 \approx 0$ and $v_{vh}/v_{Ao} = 7.25$, thus forming a 'peninsula' and a S-curl pattern. In this case, generally one appears a curve at very small dimensionless wave numbers (up to $kx_0 = 0.1$), and other two curves merging in the

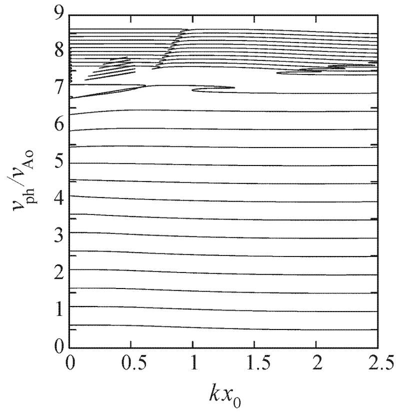

Fig. 3. Dispersion curves of forward kink waves in a forward flow for the same parameters' set as in Fig. 1

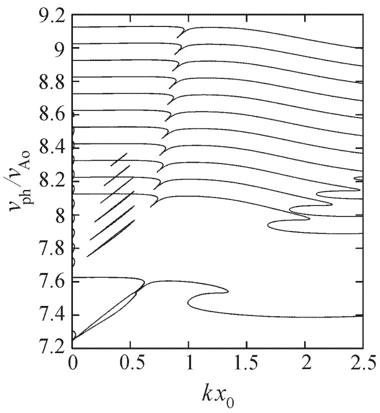

Fig. 4. Zoomed-in area of the dispersion curves for forward kink waves in a forward flow corresponding to $M_o = 6.5$ (the lowest set of curves) and to $M_o = 7$–8 (the remaining curves)

range $kx_0 = 0.6$–1.0 with a S-shaped curl at large wave numbers and isle-shaped features that occur only for $M_o = 7.0$–7.5, or in terms of the external Alfvénic Mach number—$M_e = 3.92$–4.48 (when eventually the 'peninsula'-shaped feature transforms into an 'isle'-one). The backward kink waves, however do not show any significant complication in their dispersion curves with increasing the Alfvénic Mach numbers as it is seen from Fig. 5.

BACKWARD FLOW

For the case of a backward flow we interchange the aforementioned values of the two velocities, notably setting $U_o = 420$ km s^{-1}, whilst $U_e = 480$ km s^{-1}. This leads to Alfvénic Mach numbers accordingly $M_o = 6.56$ inside the slab and $M_e = 4.8$ outside the slab. With the so-chosen magnitudes for the flow velocities the value of the relative flow speed becomes -60 km s^{-1}. The negative sign denotes the opposite direction of the relative flow velocity with respect to the direction of the magnetic field. In this case we have forward and backward sausage and forward and backward kink waves along a backward flowing flux tube.

Sausage waves in a backward flow

Here, as before, the both types of the sausage wave do not show any complications in their dispersion curves with increasing the Alfvénic Mach numbers. The forward sausage waves (Fig. 6) are directed along the positive z axis, which means they are running in opposite direction of the relative flow velocity. The plot shows a slow dispersion in the long wavelength limit (small wave numbers). Fig. 7 illustrates the behaviour of the backward sausage mode. Here again dispersion curves in the range of M_o from 6 to 7 and M_e from 4.38 to 5.11 (corresponding

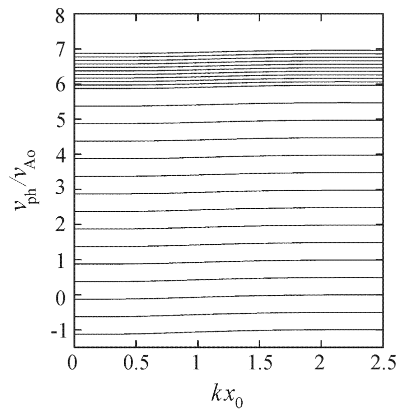

Fig. 5. Dispersion curves of backward kink waves in a forward flow for the same parameters' set as in Fig. 1

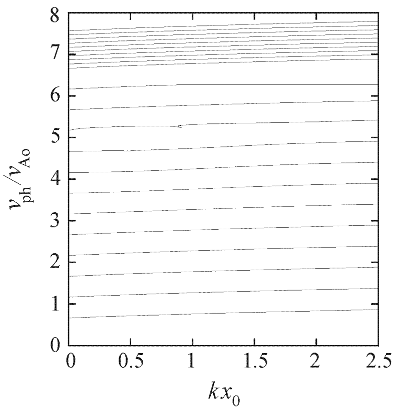

Fig. 6. Dispersion curves of forward sausage waves in a backward flow for $M_o = 0$–6 ($M_e = 0$–4.38) by a step of 0.5 and from 6 to 7 (4.38 to 5.11) with a step of 0.1. The other entry parameters are the same as in Fig. 1

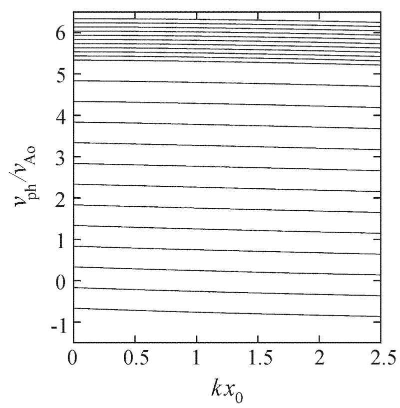

Fig. 7. Dispersion curves of backward sausage waves in a backward flow for the same parameters' set as in Fig. 6

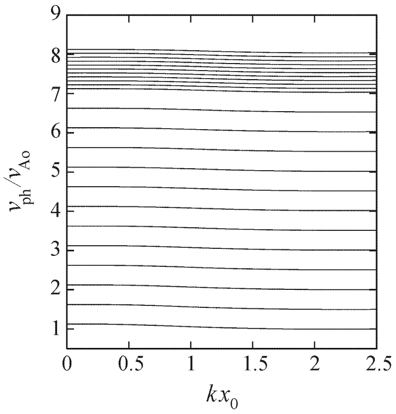

Fig. 8. Dispersion curves of forward kink waves in a backward flow for the same parameters' set as in Fig. 6

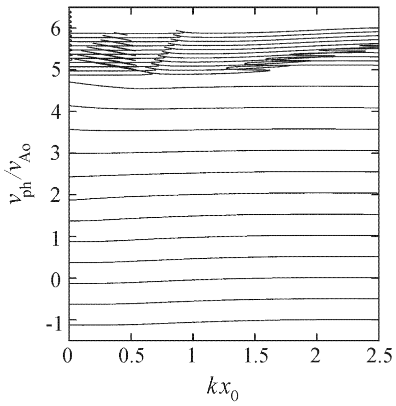

Fig. 9. Dispersion curves of backward kink waves in a backward flow for the same parameters' set as in Fig. 6

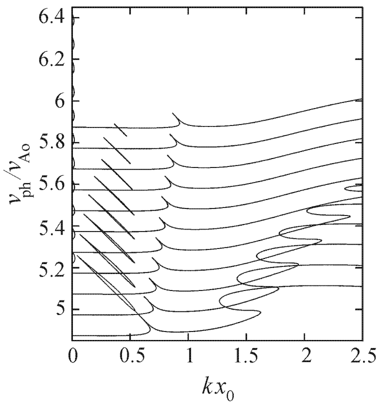

Fig. 10. Zoomed-in area of the dispersion curves for the backward kink waves in a backward flow for $M_o = 6{-}7$

to normalized phase velocity from 5.5 to 6.5) possess diminished $v_{\rm vh}/v_{\rm Ao}$s and as a whole are advected with the external flow, i.e. for an observer in the co-moving frame of reference they are becoming practically forward waves.

Kink waves in a backward flow

The forward kink waves in a backward flow are aligned smoothly, as it is seen in Fig. 8. The backward kink waves exhibit the similar complexity as do the forward kink waves propagating along a forward flow. The dispersion curves possess the same features, although being 'mirror-reversed' (Fig. 9), more specifically, an occurrence of a curve at small wave numbers and other two curves merging in the range of $|k|x_0$ between 0.5 and 1.0 with the specific S-curls and isles. We notice that the last two peculiarities retain their existence throughout the whole range of dimensionless phase velocities between 4.8 and 6.4—see Fig. 10.

DISCUSSIONS AND CONCLUSION

The dispersion properties of the obtained Hall-MHD surface waves can be summarized in the following manner. Generally the flow increases the phase velocity of the waves, transforming the initially Alfvén waves (without flow) into super-Alfvénic ones. For the backward waves the situation is somewhat different. The wave modes are *actually* backward only for small Mach numbers. Moreover, with increasing the magnitude of the flow speed, the phase velocity reduces, passes the zero and starts to increase. This corresponds to an overturning the direction of the waves' propagation, which from backward waves become forward ones with a diminished phase velocity in comparison with that of the true forward waves. The shift of the phase velocity of a particular forward/backward Hall-MHD surface wave may be expressed in the following way [7]:

$$v_{\rm ph} \equiv \frac{\omega}{k} = \frac{\rho_{\rm o}}{\rho_{\rm o} + \rho_{\rm e}}\, U_0 \pm v_{\rm ph}^{\text{Hall-MHD}}, \tag{12}$$

where U_0 is the relative flow velocity, $v_{\rm ph}^{\text{Hall-MHD}}$ is the phase velocity of the wave in a static plasma configuration and the $\pm$ sign denotes a forward/backward wave. The above equation is in concordance with Eq. (31) in Ref. [2], which is however relevant to unbounded Hall-MHD plasmas and as a result of this circumstance the coefficient in front of U_0 is simply 1. Apparently when the flow velocity is larger than the $v_{\rm ph}^{\text{Hall-MHD}}$ (the present case), the phase velocity of the wave in a flowing plasma slab is determined mainly on the speed of the flow and the waves are advected in this flow.

As we have already mentioned, the transfer structure of the obtained sausage and kink surface waves is determined by two pairs of attenuation coefficients, $\kappa_{\rm o1,2}$ and $\kappa_{\rm e1,2}$. In the most cases one of the $\kappa_{\rm o,e}$ s is real and the other is imaginary. Moreover, the increasing of the dimensionless wave number kx_0 leads to changes in the attenuation coefficients' magnitudes, that corresponds to a variation in the transfer structure of the wave. Generally, the Hall-MHD waves are a mixture of the main types of waves: pure surface, pseudo-surface and leaky ones. The exact determination of the transfer structure of all considered surface waves is however a tough but generally solvable task that needs an individual treatment.

Another important aspect of this study is related to the five entry parameters. During the numerical solving we kept three of them unaltered (the plasma β, the plasma density ratio $\rho_{\rm o}/\rho_{\rm e}$ and the parameter $l_{\rm Hall}/x_0$), whereas the two Alfvénic Mach numbers were allowed to grow. A reasonable question that can arise is what might occur if one of the unchanged entry parameters varies. For small variation in β near 1 the shapes of the dispersion curves remain similar to the obtained ones. The same is true for any small deviation in the chosen value of $l_{\rm Hall}/x_0$. The magnitude of the density ratio is restricted by Eq. (11) as we pointed out previously. For any drastic change in those parameters however it is naturally to expect a considerable modification of dispersion curves' shape that is especially noticeable for significant variations of the plasma β.

As we have mentioned above, the changing of the wave number k leads to an alteration of the dispersion attenuation coefficients $\kappa_{1,2}$, which being real quantities for some ks (and corresponding to pure surface waves) later on, for other ks, become imaginary (associated with pseudo-surface or leaky waves). This implies that for imaginary κs the hyperbolic functions tanh and coth in dispersion relations transform into periodic ones tan and cot, respectively. This is the reason for the appearance of *harmonic* dispersion curves together with the *fundamental* curves in the dispersion diagrams [11]. To simplify the plots we have presented only the fundamental solutions for each of the considered cases.

Another tough aspect of this study is the question of the stability of the Hall-MHD wave modes travelling in bounded plasma tubes. Because of the extremely complexity of the obtained dispersion relations, the applicability of the existing criteria for stability needs a separate treatment which is beyond the scope of this work. In any case, the Kelvin–Helmholtz and resonant flow instabilities [12,13] may play a principal role in the MHD dissipation mechanisms, or in the process of amplification of the waves, as well as in the driving of a MHD turbulence in the solar wind.

Finally we came to the main point of this work—the possibility for any real application of our flow-tube model. The problem of the propagation of the different plasma waves in solar-wind flow structures is already considered in a large number of papers (see Refs. [14,15] and bibliography therein). There, the influence of the fast (together with intermediate) wave modes has been investigated alongside the more general case of oblique wave propagation in the framework of the conventional MHD approach. The Hall case has been treated in Refs. [6,11,16], where the authors consider the simpler plasma configuration of a static flux tube embedded in a constant in all space magnetic field $\boldsymbol{B}_0$. A more realistic model, however, would consider the presence of different magnetic fields inside and outside the slab, as well as different plasma densities and flow velocities, which is consistent with the observational data. Moreover, the presence of sharp borders in the real structures is doubtful and is unlikely to happen. That is why it is necessary to investigate the effects of any present density gradients and shear flows observed in such a bounded plasma slab. A further improvement of the present flow-structured model, which is in progress and will be reported elsewhere, is oriented towards the aforementioned remarks.

Acknowledgments: The authors are indebted to Dr. Mon'o Kartalev for discussing the appropriate magnitudes of plasma and flux tube characteristics of the solar wind at 1 AU.

APPENDIX

The full expression of the dispersion relation for sausage and kink modes is:

$$\tilde{\omega}\left\{\frac{k^2}{q_{\rm o}^2}\left[\left(\frac{\omega-\boldsymbol{k}\cdot\boldsymbol{U}_{\rm o}}{kv_{\rm Ao}}\right)^2-1\right]\left(-Y_0\,\kappa_{\rm o1}\begin{pmatrix}\coth\\ \tanh\end{pmatrix}\kappa_{\rm o1}x_0+\kappa_{\rm o2}\begin{pmatrix}\coth\\ \tanh\end{pmatrix}\kappa_{\rm o2}x_0\right)\right\}$$

$$+\frac{k^2}{q_{\rm e}^2}\left[\left(\frac{\omega-\boldsymbol{k}\cdot\boldsymbol{U}_{\rm e}}{kv_{\rm Ae}}\right)^2-1\right]\frac{1}{(G_{\rm e1}-G_{\rm e2})}\left\{\kappa_{\rm e1}\left[G_{\rm o2}-\tilde{\omega}G_{\rm e2}-(G_{\rm o1}-\tilde{\omega}G_{\rm e2})\,Y_0\right]\right.$$

$$\left.-\,\kappa_{\rm e2}\left[G_{\rm o2}-\tilde{\omega}G_{\rm e1}-(G_{\rm o1}-\tilde{\omega}G_{\rm e1})\,Y_0\right]\right\}$$

$$-\,\varepsilon_{\rm e}\left[\left(-Y_0\,G_{\rm o1}\,\kappa_{\rm o1}\begin{pmatrix}\coth\\ \tanh\end{pmatrix}\kappa_{\rm o1}x_0+G_{\rm o2}\,\kappa_{\rm o2}\begin{pmatrix}\coth\\ \tanh\end{pmatrix}\kappa_{\rm o2}x_0\right)\right.$$

$$+\frac{1}{G_{\rm e1}-G_{\rm e2}}\left\{\kappa_{\rm e1}\,G_{\rm e1}\left[G_{\rm o2}-\tilde{\omega}G_{\rm e2}-(G_{\rm o1}-\tilde{\omega}G_{\rm e2})\,Y_0\right]\right.$$

$$- \kappa_{e2} G_{e2} [G_{o2} - \tilde{\omega} G_{e1} - (G_{o1} - \tilde{\omega} G_{e1}) Y_0]\} \Big] = 0,$$

where

$$\tilde{\omega} = \frac{\omega - \boldsymbol{k} \cdot \boldsymbol{U}_e}{\omega - \boldsymbol{k} \cdot \boldsymbol{U}_o}, \qquad \varepsilon_{o,e} = \frac{\omega - \boldsymbol{k} \cdot \boldsymbol{U}_{o,e}}{\omega_{ci}}, \qquad Y_0 = \frac{1 - CG_{o2}}{1 - CG_{o1}},$$

and

$$C = \frac{1}{\varepsilon_o} \left(\frac{\omega - \boldsymbol{k} \cdot \boldsymbol{U}_o}{k v_{Ao}} \right)^2 \frac{1 - \tilde{\omega}/(\rho_o/\rho_e)^2}{1 - \tilde{\omega}/(\rho_o/\rho_e)} - \varepsilon_o.$$

REFERENCES

1. Parker, E. N. Interplanetary Dynamical Processes, Interscience, New York, 1963.
2. Vocks, C., U. Motschmann, K.-H. Glassmeier. *Ann. Geophysicae*, **17**, 1999, 712.
3. Huba, J. D. *Phys. Plasmas*, **2**, 1995, 2504.
4. Tu, C.-Y., E. Marsh. *Space Sci. Rev.*, **73**, 1995, 1.
5. Nakariakov, V. M., B. Roberts. *Sol. Phys.*, **159**, 1995, 213.
6. Zhelyazkov, I., A. Debosscher, M. Goossens. *Phys. Plasmas*, **3**, 1996, 4346.
7. Chandrasekhar, S. Hydrodynamic and Hydromagnetic Stability, Oxford University Press, Oxford, 1961.
8. Swanson, D. G. Plasma Waves, Academic Press, San Diego, 1989.
9. Edwin, P. M., B. Roberts. *Sol. Phys.*, **76**, 1982, 239.
10. Cravens, T. E. Physics of Solar System Plasmas, Cambridge University Press, Cambridge, 1997, chaps. 5&6.
11. Zhelyazkov, I., G. Mann. *Contr. Plasma Phys.*, **40**, 2000, 569.
12. Tirry, W. J., V. M. Čadež, R. Erdélyi, M. Goosens. *Astron. Astrophys.*, **332**, 1998, 786.
13. Taroyan, Y., R. Erdélyi. *Phys. Plasmas*, **9**, 2002, 3121.
14. Nakariakov, V. M., B. Roberts, G. Mann. *Astron. Astrophys.*, **311**, 1996, 311.
15. Joarder, P. S. *A&A*, **384**, 2002, 1086.
16. Zhelyazkov, I., G. Mann. *Phys. Plasmas*, **10**, 2003, 484.

Received March 2003

Rossitsa Miteva
St. Kliment Ohridski University of Sofia
Faculty of Physics
Department of Radiophysics and Electronics
5 James Bourchier Blvd.
BG-1164 Sofia, Bulgaria
E-mail: rmiteva@phys.uni-sofia.bg